(a) (b)

Fig. 1. Reference markers on the (a) fluoroscope and (b) pelvis.

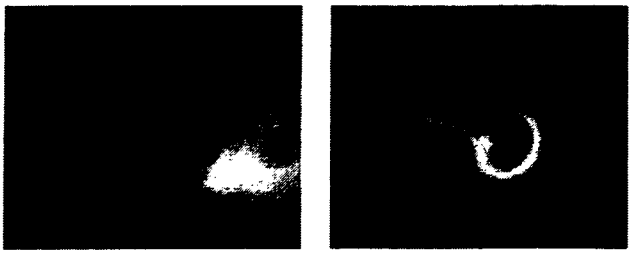

(a) (b)

Fig. 2. DRRs for simulation. (a) Original volume. (b) Segmented volume (proximal fragment only).

where $dist(\cdot)$ is the Euclidean distance between two points, and p'_{rc} and p_{rc} are the hip rotation center assumed in computation and the position tracked by the optical localizer. Let $T_{\text{pelvis\_tracker}}$ be the latest transformation matrix of the pelvis reference marker. The tracked position can then be obtained by

$$p_{rc} = T_{\text{pelvis\_tracker}}\, {}^{\text{pelvis\_tracker}}p_{rc} \tag{2}$$

where ${}^{\text{pelvis\_tracker}}p_{rc}$ is determined by the femoral head center localization in the CT volume and the first registration step.

A hybrid similarity measure that combines the constraints given by the hip joint rotation center tracking and the 2-D/3-D registration can then be defined as

$$E_{\text{hybrid}} = -E_{\text{image}} + \gamma E_{\text{position}} \tag{3}$$

where γ is a weighting coefficient.

The optimizing computation is based on the Powell method [4]. A weighted search method [2] is employed for coarse optimization, and a polynomial function fitting method [5] is then adopted for improvement of depth accuracy.

III. Experiments

A. Image and Position Data Acquisition

CT volumes were acquired using a HiSpeed Plus scanner (General Electric Co., USA) with a voxel size of $0.68 \times 0.68 \times 1\ \text{mm}^3$ for the fractured part and the femoral head, and $0.68 \times 0.68 \times 3\ \text{mm}^3$ for other parts. Fluoroscopic images were taken intraoperatively using a Siremobil Iso-C instrument (Siemens AG, Germany). The image size was 640×512 pixels. The positions of the fluoroscope and the pelvis were obtained for each registration step using an optical localizer (Optotrak, Northern Digital Inc., Waterloo, ON, Canada). The reference markers (Fig. 1) were attached to the image intensifier cylinder of the fluoroscope and the pelvis (C-arm Tracker and VersaTrax Tracker, Traxtal Technologies Inc., Toronto, ON, Canada). The pelvis tracker shown in Fig. 1(b) can be fixed to the patient's lumbus using a silicone belt with Velcro tape for hipline length adjustment. The silicone belt has two fixation holes that fit to the anterior-superior-iliac spine around the left and right sides of the pelvis to ensure that the tracker is immobilized against the patient's body.

B. Simulations

CT images of five patients and two phantoms were used in simulations of the proposed tracking method. For use as fluoroscopic images to be input into the simulation, digitally reconstructed radiographs (DRRs) of each original CT volume were generated from arbitrary viewpoints determined so as to emulate the real dimensions of fluoroscopy during surgery. The initial positions of the fragment registration were determined by random perturbation from the original position in the CT volume. The standard deviation of the perturbation was 3 mm for translation and 3° for rotation. The overlap of bone or soft tissue in fluoroscopy hampers 2-D/3-D registration. For estimating such influences, segmented CT volumes of the fragments of the fractured femur, pelvis, and soft tissue were used in simulated fluoroscopy. The DRRs were then generated from the CT volumes of the proximal fragment and the entire abdominal structure. In DRR generation, the CT volumes of the proximal fragment were used to estimate the accuracy of principal registration, and the original CT volumes were used to estimate the overall accuracy and the influence of soft tissue overlap. Examples of DRRs are shown in Fig. 2. The error at the femoral head center was computed statistically by comparing estimated positions with the original position. For accuracy validation, 100 trials of registration were performed for each parameter set.

The results are summarized in Tables I and II. Averages, standard deviations and, worst error are shown. The estimation accuracy was affected by the overlap of soft tissue and bone. Nevertheless, the proposed method was more robust than the single-view method, and provided results closer to the real position. The component error of depth translation in the fluoroscopy coordinate system in particular was substantially improved, for example, from 1.49 mm to 0.007 mm in the case of the full abdominal patient CT. The accuracy was also found to depend on the spatial distribution of X-ray absorption in the target object. In the case of the proximal fragment bone, the distribution may have rotational symmetry around the femoral neck axis, and the maximum principal component of error variance was oriented parallel with this axis. In the phantom CT experiment, the maximum principal components of the error distribution were 2.73° and 0.80° in the single-view and proposed methods, respectively, representing contributions of 82.02% and 79.03%. After removing the maximum principal component, the residual errors were 1.28° and 0.41°, respectively. In the patient CT experiment, the maximum principal components of the error distribution were 1.06° and 0.71°, corresponding to contributions of 44.68% and 40.22%, and the residual errors were 1.18° and 0.86°, respectively.

C. In-Vitro Experiment

Two phantoms were used to simulate scenes of proximal femur fracture in an *in vitro* experiment. Plastic pelvis and femur models (Sawbones Pacific Research Laboratories, Vashon, WA) were fractured and aligned using Styrofoam plates. The alignment of the fractured fragments was determined based on a typical intertrochanteric fracture. To find the "gold standard" registration, four fiducial markers (30-mm glass balls) were embedded in the Styrofoam cover of the phantom, ensuring that the markers did not overlap in the pelvis and femur silhouettes in fluoroscopy. Four light-emitting diode markers were also attached to the front of the phantom Styrofoam cover as reference markers for optical tracking.

Fig. 3 shows the experiment setup, where arrows indicate the positions of reference markers. The phantom was placed on a carbon bed (Mizuho, Japan), and the positions of the fluoroscope and phantom

[7] S. Warisawa, T. Ishizuka, M. Mitsuishi, N. Sugano, K. Yonenobu, and T. Nakazawa, "Development of a femur fracture reduction robot," in *Proc. IEEE Int. Conf. Robotics and Automation (ICRA 2004)*, 2004, pp. 3999–4004.

[8] F. Ino, Y. Kawasaki, T. Tashiro, Y. Nakajima, Y. Sato, S. Tamura, and K. Hagihara, "A parallel implementation of 2-D/3-D image registration for computer-assisted surgery," *Int. J. Bioinformatics Res. Appl.*, vol. 2, no. 4, pp. 341–358, 2006.

Redefining Performance Evaluation Tools for Real-Time QRS Complex Classification Systems

Philippe Ravier*, Frédéric Leclerc, Cedric Dumez-Viou, and Guy Lamarque

***Abstract*—In a heartbeat classification procedure, the detection of QRS complex waveforms is necessary. In many studies, this heartbeat extraction function is not considered: the inputs of the classifier are assumed to be correctly identified. This communication aims to redefine classical performance evaluation tools in entire QRS complex classification systems and to evaluate the effects induced by QRS detection errors on the performance of heartbeat classification processing (normal versus abnormal). Performance statistics are given and discussed considering the MIT/BIH database records that are replayed on a real-time classification system composed of the classical detector proposed by Hamilton and Tompkins, followed by a neural-network classifier. This study shows that a classification accuracy of 96.72% falls to 94.90% when a drop of 1.78% error rate is introduced in the detector quality. This corresponds to an increase of about 50% bad classifications.**

***Index Terms*—Classification, hardware implementation, heartbeat recognition, neural network, QRS complex detection.**

I. Introduction

The problem of heartbeat classification has been widely explored in the literature [1]–[8]. However, real-time classification systems often necessitate the detection of the cardiac beats before any classification procedure. The cardiac beats are also refered to QRS complex shapes where the letters stand for the three successive main phases of a cardiac cycle. In such classification systems, classical performance evaluation tools become irrelevant since the detection errors are not taken into account in the classification statistics. In this communication, we therefore propose to:

- redefine the classical performance evaluation tools taking the entire classification system into consideration;
- experimentally discuss the influence of the detection stage on classification results;
- give material for finding the best compromise between the quality of the detector, the quality of the classifier, and the computational time in real-time classification systems.

In order to achieve these goals, we implemented a simple real-time classification system on an electronic board. The proposed system is composed of a QRS complex extractor (detection part) followed by a normal or abnormal peak recognition step (classification part). Abnormal beats are opposed to normal beats according to their QRS waveform shapes.

For instance, a normal/abnormal classification system may be useful for Holter monitoring where only the critical parts as well as the cardiac history (i.e., peak-to-peak intervals) are of medical interest. It is not worth recording the healthy electrocardiographic (ECG) samples. The amount of data can therefore be drastically reduced and the entire breakdown will be shorter since the physician will devote his or her expertise to the critical parts of the ECG signal, while also taking into account the peak-to-peak intervals of the entire monitoring.

Several algorithms have been proposed in the literature for the detection and classification of ECG beats. Since our system has to be embedded with real-time processing constraints, the computation cost must be low. Various approaches (wavelets [9], [10]; filter banks [11]; and neural networks [12]) have been investigated to improve the quality of the detectors. However, the gain obtained is generally offset by the greater complexity of the algorithms, involving higher computational costs. It is the reason why the well-known Hamilton and Tompkins [13], [14] detector has been chosen here. Similarly, many methods have been investigated for the classification part (neural networks [1]–[3], fuzzy theory [3], [5], support vector machine [4], higher order spectral techniques [6], and hidden Markov models [7], ...). A neural-network approach has been adopted in this study because its parallel processing implementation is well adapted to real-time constraints. Finally, we tested the system on the Massachusetts Institute of Technology–Beth Israel Hospital Arrythmia Database (MIT–BIH) [15] since this database is commonly used for performance evaluations of detection or classification algorithms.

This communication is organized as follows. The classification system is introduced in the second part. Such a system leads to the redefinition of the performance evaluation tools in the third part. These new tools are tested on real data in the fourth part, considering real-time classification of the MIT/BIH recordings. The communication ends with discussions and conclusions.

II. Normal/Abnormal Real-Time Beat Classification System

After digitizing the analog ECG signal through a 16–b analog-to-digital converter (ADC) using a 360-Hz sampling rate, the algorithmic part is divided into two main functions (Fig. 1).

1) The ECG beat extractor detects QRS complex waveforms and extracts ECG waveform patterns after they have been normalized and centered about the fiducial point. Two versions of the Hamilton and Tompkins detector have been real time implemented [13], [14]: the first one includes the search back procedure (SB+) and the second one does not (SB−).
2) the neural-network classifier that is fed by Fourier coefficients of the ECG waveform patterns provided by the previous stage. The classifier is a multilayer perceptron (MLP) [16] with 16 input nodes (16 first absolute values of the 128 Fourier samples excluding the dc component), four neurons in the hidden layer, and one output neuron. Each neuron labeled 1 to 5 has four inputs and one output with the classical associated sigmoidal activation function $y_j(n) = (1)/(1 + e^{-v_j(n)+w_j})$, where n is the number of QRS pattern to be classified and j is the neuron number. The value $v_j(n)$ is the net internal activity level of neuron j and is equal to $v_j(n) = \sum_{i=1}^{4} w_{ji} x_{ji}(n)$, for $j = 1$ to 4 and $v_5(n) =$

Manuscript received May 12, 2006; revised December 18, 2006. *Asterisk indicates corresponding author.*

P. Ravier is with the Laboratory of Electronics, Signals and Images, University of Orleans, Orléans Cedex 45067, France (e-mail: philippe.ravier@univ-orleans.fr).

C. Dumez-Viou and G. Lamarque are with the Laboratory of Electronics, Signals and Images, University of Orleans, Orléans Cedex 45067, France (e-mail: cedric.dumez-viou@obs-nancay.fr; guy.lamarque@univ-orleans.fr).

F. Leclerc is with the Laboratory of Electronics, Signals and Images, University of Orleans, Orléans Cedex 45067, France and also with the Department of Aerospace Physiology, Institute of Aerospace Medicine of the Army Health Department, Brétigny-Sur-Orge Cedex 91223, France (e-mail: frederic.leclerc@univ-orleans.fr).

Digital Object Identifier 10.1109/TBME.2007.902594

TABLE I
ESTIMATION ERROR FOR TRANSLATION IN SIMULATION

	Phantom [mm] (proximal fragment only)	Phantom [mm]	Patient [mm] (proximal fragment only)	Patient [mm]
Single-view method	0.12±0.32 (1.03)	1.07±2.76 (11.314)	0.0061±0.27 (0.74)	1.91±2.43 (8.29)
Proposed method	0.00047±0.013 (0.11)	0.044±0.058 (0.21)	0.00046±0.0061 (0.029)	0.51±0.30 (0.86)

TABLE II
ESTIMATION ERROR FOR ORIENTATION IN SIMULATION

	Phantom [degrees] (proximal fragment only)	Phantom [degrees]	Patient [degrees] (proximal fragment only)	Patient [degrees]
Single-view method	0.18±1.11 (3.243)	1.40±3.02 (10.2)	0.0068±0.15 (0.41)	1.80±1.59 (5.37)
Proposed method	0.10±0.96 (2.92)	2.55±0.90 (5.06)	0.075±0.98 (1.90)	1.47±1.11 (3.45)

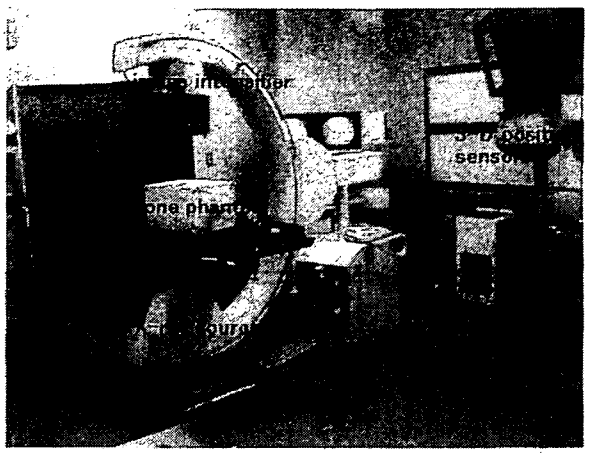

Fig. 3. *In vitro* experiment setup.

TABLE III
ESTIMATION ERROR IN IN VITRO PHANTOM TEST

	Translation error [mm]	Orientation error [degrees]
Single-view method	2.52±2.02 (10.41)	2.54±1.92 (6.32)
Proposed method	1.83±0.51 (3.37)	1.29±1.70 (4.23)

were localized using an optical sensor. The phantom reference marker was used as the reference marker for the pelvis, and also to track the rotation center of the hip joint. Fluoroscopy was performed simultaneously.

The errors are summarized in Table III. The translation error was successfully improved by applying the proposed method. The maximum principal components of error variance for rotation were 1.58° and 1.45° for the single-view and proposed methods, representing contributions of 50.97% and 72.35%, respectively. The remaining error was 1.55° and 0.89°, respectively.

IV. DISCUSSION

Although some of the worst case results appear to have converged at local minima and are not clinically acceptable, most of the results converged to acceptable values. In our experiments, the convergence behavior from initial bone positions was predictable in most cases, and manual adjustment of the initial position corrected the result.

The bias error in the *in vitro* phantom test was greater than that indicated by the simulations. This can be primarily attributed to positional error in optical tracking, and is also a result of the use of DRRs as input images in the simulation, whereas real fluoroscopic images were used in the *in vitro* test.

The overlap of soft tissue and other bones resulted in the appearance of untrue edges in the CT volumes. In the single-view method, convergence to local minima is caused in part by the overlap of other anatomical structures, particularly the edge of the pelvis acetabular. The proposed method avoids this effect and achieves successful registration in such situations, primarily as a result of the positional constraint imparted by hip rotational center tracking.

As the constraint E_{position} effectively compensates for the positional inaccuracy in E_{image}, 2-D/3-D registration accuracy is improved by the proposed method, particularly with respect to depth. This approach does not require interactive C-arm re-positioning, and therefore will be advantageous for reducing the time required for fracture reduction by robotic surgery [7].

For real-time bone tracking, registration should be performed at least 30 times/second. The computation time for the proposed method at present is 300 s/registration by a PC (Xeon 3.2 MHz CPU, 2 GB memory), and less than 10 s when computed on a parallel platform consisting of 128 CPUs [8]. Therefore, some supplemental technologies are required in order to introduce robotic surgery into practical clinical settings. The robotic manipulators should move slowly for safety, and some form of prediction (or extrapolation) techniques should be introduced for bone motion to reduce imaging frequency. As the method requires frequent imaging, the X-ray exposure dose to both the patient and surgeons must also be considered. The Siremobil Iso-C instrument employed for pulse-mode fluoroscopy emits a strong but instantaneous X-ray pulse that affords good-quality images at a reduced total X-ray dose compared to continuous fluoroscopy. The X-ray dose for the present procedure is 0.92 mGy/min with imaging at 1 Hz, less than a half that of regular fluoroscopy (2.38 mGy/min).

REFERENCES

[1] S. Lavallée and R. Szeliski, "Recovering the position and orientation of free-form objects from image contours using 3D distance map," *IEEE Trans. Pattern Anal. Mach. Intell.*, vol. 17, no. 4, pp. 378–390, Apr. 1995.

[2] J. Weese, G. P. Penney, P. Desmedt, T. M. Buzug, D. L. G. Hill, and D. J. Hawkes, "Voxel-based 2-D/3-D registration of fluoroscopy images and CT scans for image-guided surgery," *IEEE Trans. Inf. Technol. Biomed.*, vol. 1, no. 4, pp. 284–293, Dec. 1997.

[3] D. B. Russakoff, T. Rohlfing, R. Shahidi, D. H. Kim, J. R. Adler Jr., and C. R. Maurer Jr., "Intensity-based 2D-3D spine image registration incorporating one fiducial marker," in *Proc. Medical Image Computing and Computer-Assisted Intervention (MICCAI) 2003*, vol. 2878, Springer LNCS, pp. 287–294.

[4] M. J. D. Powell, "An efficient method for finding the minimum of a function of several variables without calculating derivatives," *Comput. J.*, vol. 7, pp. 155–162, 1964.

[5] T. Yamazaki, T. Watanabe, Y. Nakajima, K. Sugamoto, T. Tomita, H. Yoshikawa, and S. Tamura, "Improvement of depth position in 2-D/3-D registration of knee implants using single-plane fluoroscopy," *IEEE Trans. Med. Imag.*, vol. 23, no. 5, pp. 602–612, May 2004.

[6] J. M. Fitzpatrick, J. B. West, and C. R. Maurer Jr., "Predicting error in rigid-body point-based registration," *IEEE Trans. Med. Imag.*, vol. 17, no. 5, pp. 694–702, Oct. 1998.

P2-06

直達式骨折整復を支援する骨折整復システムの開発

鄭　常賢[1]、加門　大和[1]、廖　洪恩[2]、光石　衛[2]、中島　義和[2]、
小山　毅[4]、菅野　伸彦[4]、前田　ゆき[5]、別所　雅彦[3]、大橋　暁[3]、松本　卓也[3]、
岩城　純一郎[6]、中沢　東治[6]、大西　五三男[3]、中村　耕三[3]、佐久間　一郎[2]
東京大学大学院｛[1]新領域創成科学研究科、[2]工学系研究科、[3]医学系研究科｝
[4]大阪大学大学院　医学系研究科、[5]大阪南医療センター、[6]THK(株)

骨粗鬆症がある患者におこりやすい骨折のなかでも大腿骨頚部骨折は寝たきりとなる可能性の高い骨折である。社会の高齢化の進行に伴い骨粗鬆症の患者が増加すると、大腿骨頚部骨折の患者も増加すると予測されている。

大腿骨頚部骨折の治療法は外科的な手術によるものがほとんどである。手術では大腿骨の遠位骨片を牽引しながら位置決めし、ピンによって固定する。しかし、大腿筋などの周辺組織が萎縮した状態では整復のための牽引に大きな力が必要となるため術者にとって負担となる。また、X線透視下で2次元の情報を用いて位置決めを行わなければならないため、術者の熟練が必要であり、手術を行うことで術者が受けるX線被爆も問題である。

これらの問題に対し、我々は骨折整復システムの開発を行った(Fig. 1)。システムは骨折整復ロボットとナビゲーションシステムに構成されている。骨折整復には、足首をつかみ遠位骨片の位置を合わせる介達式骨折整復方法と、骨片にピンを打ち、ピンに連結されたリングを持って直接整復を行う直達式骨折整復方法がある。骨折整復システムは介達式骨折整復に対して使えるように構成されているが、ロボットを使う利点を考えると骨片の正確な位置決めが可能な直達式骨折整復にも使用されるように構成する必要があり、今回は新たに直達式骨折整復を直達式骨折整復ロボットに実装を行った。

骨折整復ロボットは並進3自由度と回転3自由度の6自由度を有する。骨片の牽引と回旋をするときの整復力が設定値より大きくなると各関連軸をフリーにするフェイルセイフ装置が装着されており安全性を保つ。動作モードはタッチパネルを用いたジョグモード、術者の整復力をパワーアシストする手動モード、ナビゲーションからの指令により自動で整復を行う自動整復モードがある。

直達式整復では、骨とロボットの手先は専用のジグで繋がっているので、骨の長軸とロボットの牽引軸が一致しない。骨片の姿勢だけを変えるため、骨折断面の中心を仮想中心と見なし、ロボットを制御する拘束パワーアシストを実装し、有効性を検証した。

ナビゲーションシステムは術前にCTからの3次元モデルを用いて整復ゴールを計算する。術中にはC-armで撮った画像と3次元モデルをレジストレーションすることにより、実空間での骨片間の位置関係を認知する。骨片の現在位置からゴールまでの整復パスは術者の意見を反映して作成され、整復ロボットに指令を送り整復を行う。構成したシステムは骨折モデルでの整復実験でその有効性を示す。

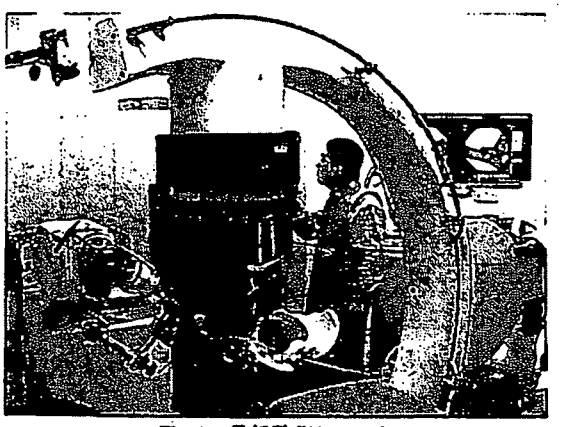

Fig.1. 骨折整復システム

07(IV)-19

直達式骨折整復の臨床データ取得システム

○ 鄭 常賢[a], 廖洪恩[b], 小林英津子[b], 光石衛[b], 中島義和[b], 小山毅[d], 菅野伸彦[d], 前田ゆき[e], 別所雅彦[c], 大橋暁[c], 松本卓也[c], 大西五三男[c], 佐久間一郎[b]

東京大学大学院{[a]新領域創成科学研究科, [b]工学系研究科, [c]医学系研究科}, [d]大阪大学大学院医学系研究科, [e]大阪南医療センター

A Clinical Data logging system of Direct fracture reduction.

S.Joung[a], H.Liao[b], E.Kobayashi[b], M.Mitsuishi[b], Y.Nakajima[b], T.Koyama[d], N.Sugano[d], Y.Maeda[e], M.Bessho[c], A.Ohashi[c], T.Matsumoto[c], I.Ohnishi[c], I.Sakuma[b]

{[a]Graduate School of Frontier Sciences, [b]Graduate School of Engineering, [c]Graduate School of Medicine}, the University of Tokyo,

[d]Graduate School of Medicine, Osaka University, [e]National Organization Osaka Minami Medical Center

Abstract: Clinical data quantification of a fracture reduction has become important as the development of new fracture reduction technology such as navigation and robot assisted fracture reduction. A reduction force and a reduction path are the key points in considering the control and safety of these new reduction methods. We have developed a clinical data logging system(CDLS) of direct fracture reduction, which reduces using ring-frame connected bone fragment directly. The CDLS synchronously records the reduction force, the reduction path and two video signals. One records the images from C-arm and the other records whole surgery process. This paper introduces the structure of CLDS and the resultants of application to fracture model.

Key words: Clinical data, Fracture reduction, Reduction force, Reduction path.

1. 序論

骨折治療は近年大きく発展してきており, 低侵襲で整復の精度を上げることが可能となってきた. 特に最近は, 術中に骨片の位置が認知できるナビゲーションシステムを用いた治療方法に関する研究が盛んに行われている [1]. 骨折治療法は様々であるが, どの治療法でも整復を伴い整復の結果が治療の成果に大きく影響する. 大腿骨頚部骨折の整復に関しては大きい整復力が必要で術者への負担が過大になる. そこで, ロボットを用いた整復支援システムに関する研究が報告されている [2, 3]. このような整復支援ロボットには過渡の整復力を防ぐための安全装置が装着されている. 一定以上の整復力が働いたときにその軸がフリー状態になるフェイルセイフ装置が一例である[3].

ロボットの制御方法と安全装置の仕様を決めるためには, 整復手術中の整復パス, 整復力などの臨床データを参照するべきであり, 今までは大きく必要とされていなかった骨折整復術中の臨床データを記録し定量化する必要性が整復技術の発展と共に高くなってきた. このため, Thomas らは整復力を定量化した[4]. しかし, 整復パスを記録していないため骨片の位置と整復力との関係は解析されていない. そこで我々は骨片に打ったピンをリングフレームで固定し, そのフレームを持ち骨折整復を行う直達式整復術中の整復力とパスを記録するシステムを開発した[5]. しかし, 整復力を計測するセンサの滅菌を検討してなかったので, 臨床使用には適してなかった. 本研究では, 臨床使用可能とするように改良し, さらに画像入力も可能としたシステムを紹介し, 模擬骨を用いた整復への応用結果を報告する.

2. 臨床データ取得システム

臨床データ取得システム(Clinical Data loggings system, CDLS)では骨折整復時に発生する整復力, 整復パス, C-arm画像と現場の様子を記録することが望ましい. 我々の開発した CDLS は, PC,画像入力ボード (PCI-5531, Interface), 整復力を測るための力覚センサ (IFS-67M25T50, Nitta, 定格 Fx, Fy [N]: 450; Fz [N]: 900; Mx - Mz [Nm]:40), 整復パスを追跡するための光学式 3 次元位置計測装置(Polaris, NDI, Canada)で構成され, 以上のデータを計測可能とした. これらのデータは位置と整復力との関係などを分析するため, 同期を取って記録する必要があり, システムではひとつのプロセスでコンピュータ側からデータ要求信号を送りそのときのデータを取得する方法を用いた.

Thomasらの研究結果によると骨片の牽引力の最大値は396N, 回旋トルクの最大値は74Nmなので使用した力覚センサの定格は十分である. しかし, 力センサの適切な滅菌法がないため, 滅菌可能なカバーを製作した. カバーはアシスタントの補助により, 術者の手を汚すことなく, 取り付けられる. Fig. 1にカバーを取り付けた力覚センサと整復装置の外観を示す. 図の右はカバーを外したときのセンサとカバーの様子である. カバーには整復パスを記録するため, 光学式 3 次元位置計測装置のマーカを付着した. 骨片の位置と整復力を計算するための概念図を

Fig. 2 に示す. 光学式 3 次元位置計測装置, 力覚センサ, C-armと骨片の座標系を各々ΣP, ΣS, ΣC, ΣBと設定する. ΣPからΣSとΣC への変換行列 ${}^{P}T_{S}$ と ${}^{P}T_{C}$ は 3 次元計測器から計測できる. ΣC からΣBへの変換行列 ${}^{C}T_{B}$ は 2D/3D レジストレーションなどの手法で求められる. 以上の変換行列で力覚センサの座標系から骨座標系への変換行列 ${}^{S}T_{B}$ が式(1)で計算できる.

$$ {}^{S}T_{B} = \left({}^{P}T_{S}\right)^{-1} {}^{P}T_{C}\, {}^{C}T_{B} \tag{1} $$

そこで骨片と整復装置を剛体として考えると, ${}^{S}T_{B}$ を一回計算しておくことにより, 整復中はセンサのマーカを追跡することたけで光学式 3 次元位置測装置から見た骨の位置と姿勢が式(2)で求められる.

$$ {}^{P}T_{B} = {}^{P}T_{S}\, {}^{S}T_{B} \tag{2} $$

整復力に関しても, 式(3)(4)により, センサから計測した力が骨座標系の力に変換できる.

$$ {}^{B}T_{S} = \left({}^{S}T_{B}\right)^{-1} = \begin{bmatrix} {}^{B}R_{S} & {}^{B}P_{S} \\ 0 & 1 \end{bmatrix} \tag{3} $$

$$ \begin{bmatrix} {}^{bone}\mathbf{f} \\ {}^{bone}\mathbf{n} \end{bmatrix} = \begin{bmatrix} {}^{B}R_{S} & \mathbf{0} \\ \left[{}^{B}P_{S}\times\right]{}^{B}R_{S} & {}^{B}R_{S} \end{bmatrix} \begin{bmatrix} {}^{sensor}\mathbf{f} \\ {}^{sensor}\mathbf{n} \end{bmatrix} \tag{4} $$

3. 骨折モデルの整復への応用

骨折モデルは X 線で確認できる材質のモデル骨を骨折させ, 筋肉代わりにゴムを貼り付けることで製作した. 大腿骨頚部骨折の場合, 骨片は中殿筋, 外閉鎖筋などの働きにより上半身のほうに引っ張られ, 外旋されるのでその働きをゴムで模擬した. 今回の実験では骨の座標はペンマーカを用いて指定した. 整復は整形外科医により行い, そのときのデータを CDLS により取得した. C-armは使わず, 代わりにカメラからの画像を入力した.

データの取得周期 0.3s で 2 枚の画像, 整復力と整復パスを記録することができた. Fig. 3 に取得した整復力を示す. 整復力はy軸の力(牽引方向)とモーメント(内旋方向)に大きく必要とすることが解る. 整復パスはマーカが術者に隠され一部記録できてない部分があった.

4. 考察と結論

実験では模擬骨を用いたので, 計測した整復力の大きさには意味がないが, どの成分の整復力が働くか確認することができた. また整復時の骨片の動きも確認することができた. センサのマーカは術者に邪魔にならない横方向に移すべきである. データ取得周期は 0.3 秒で遅いが, 整復の動作がゆっくり行われるので問題にはならない. 周期をあげるためには複数のパソコンにより並列処理をすればよいが, システムが大きくなるので手術現場では適さない.

今後は, C-armとレジストレーション方法を用いた模擬整復でシステムを評価し, 実際に臨床でデータ取得を行う予定である.

謝辞

本研究の一部は厚生労働科学研究費補助金(生体機能解析・補助・代替機器開発研究事業)(17100301)による.

文献

1) P.Grützner, et al.:"Computer aided long bone fracture treatment", Injry, Int.J.Care injured(2004) 35, S-A57-S-A64, 2004
2) B. Füchtmeier, et al.:"Reduction of femoral shaft fractures in vitro by a new developed reduction robot system 'RepoRobo'", Injury, Int.J.Care Injured (2004)35, S-A113-S-A119, 2004
3) Mamoru MITSUISHI, et al.: "Development of a Computer-Integrated Femoral Head Fracture Reduction System", Proceedings of the 2005 IEEE International Conference on Mechatronics,834-839, 2005
4) Thomas Gösing, et al.: "Force and Torque during Fracture Reduction: Intraoperative Measurements in the Femur", Journal of Orthopaedic Research, 333-338,2006
5) 森本顕二郎 他, " 直達式骨折整復支援装置に関する研究" 第15回日本コンピュータ外科学会大会論文集, 2006

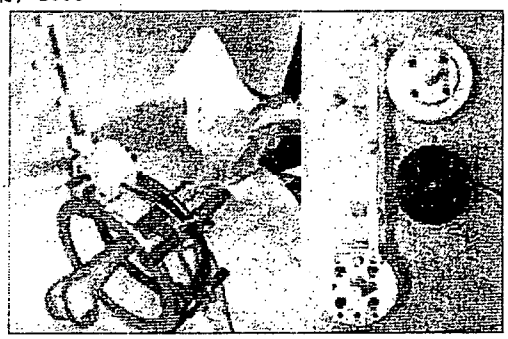

Fig. 1 Fracture reduction device.

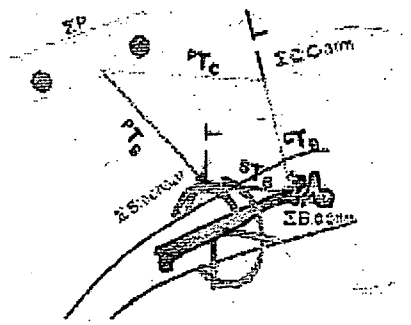

Fig. 2 Coordinate and translation matrix.

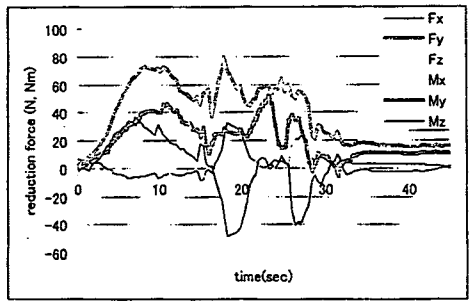

Fig.3 The reduction force during fracture reduction